Metrol. Meas. Syst., Vol. 32 (2025) No. 1, pp. 1–18
DOI: 10.24425/mms.2025.152770

PAN POLSKA AKADEMIA NAUK

METROLOGY AND MEASUREMENT SYSTEMS
Index 330930, ISSN 0860-8229
www.metrology.wat.edu.pl

M&MS

SYSTEM FOR MEASURING ELECTRIC PARAMETERS OF THERMOELECTRIC CELL BATTERY OF A SECTIONAL MODULE WITH THERMOGENERATORS

Mirosław Neska[1)], Tadeusz Opara[2)]

1) Łukasiewicz Research Network – Institute for Sustainable Technologies, K. Pułaskiego 6/10, 26-600 Radom, Poland (✉ *miroslaw.neska@itee.lukasiewicz.gov.pl*)
2) Kazimierz Pułaski University of Technology and Humanities, Stasieckiego 54, 26-600 Radom, Poland

Abstract

One way to manage low-temperature heat is to convert it directly into DC electricity using thermocells. By placing a single thermoelectric generator or a battery of thermoelectric cells between two heat exchangers, one side with a higher temperature medium and the other with a lower temperature medium, a temperature difference is created between the covers of the thermoelectric elements, which causes heat transfer and the generation of electricity. The module with thermogenerators and exchangers (MTEG) discussed in the article is equipped with a developed measurement system. This system is used to determine the electric current of twenty, serially-connected thermoelectric generators and to measure the electric voltage across the load resistance of the thermoelectric circuit. The publication presents subcircuits for measuring the internal resistance of two thermogenerators placed symmetrically in individual sections of the MTEG module. According to the developed test method, the measurement system was verified in cyclic tests with varying thermodynamic forcing. The accuracies of the test bench electric parameter measurement paths were estimated, yielding expanded uncertainties of ±0.012 W in the measurement of generated electric power and ±0.0008 Ω and ±0.0009 Ω in the resistance of the internal thermogenerators, respectively. Repeatability (EV) was verified and the "capability" of the developed measurement system to function correctly was confirmed..

Keywords: thermoelectric cell, measurement of electric parameters, measurement, uncertainty, internal resistance.

1. Introduction

Increasing energy demand, dwindling fossil fuel resources and, at the same time, concern for the environment imply the need for new initiatives, such as improving the energy efficiency of processes, increasing the use of renewable energy [1] and reducing carbon dioxide (CO_2) emissions. In particular, waste heat management could improve the energy efficiency of many processes. Some countries and their industries are a case in point, *e.g.*: in Turkey, about 41% of the total heat consumed in the manufacturing industry (cement plants) is not used [2, 3], in Serbia,

Article history: June 5, 2024; revised September 5, 2024; accepted September 14, 2024; available online November 11, 2024.

about 45% of heat is lost in industrial installations [4], and in France it is estimated that about 30% of heat energy is unused and lost in the form of hot flue gases, cooling water and heated product [5].

One method of managing waste heat is its conversion to electricity using thermoelectric cells and the Seebeck phenomenon [6]. Thermoelectric cells in a single *thermoelectric generator* (TEG) are usually connected in series, and entire TEG components are connected serially or parallelly to form larger thermoelectric generator sets/batteries [7]. A thermoelectric generator generates electricity when temperature difference ΔT between its opposite walls is caused by a hot temperature on one wall and a low temperature on the other [8]. This technology has so far been used more widely in medical, military and space solutions [9–11]. The structure of such an element and its electric circuit is shown in Fig. 1.

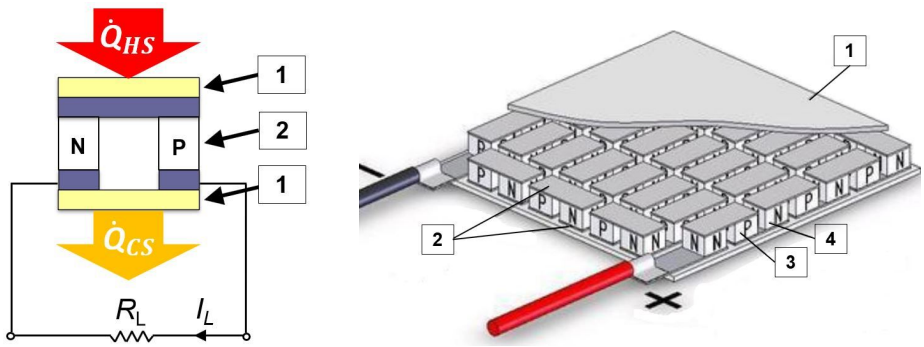

(a) (b)

Fig. 1. Thermogenerator design; a) electric circuit (1 – ceramic cover, 2 – inner layer of semiconductors type N and P, $\dot{Q}$ – heat flux); b) view of the semiconductor layer (1 – ceramic cover, 2 – copper conductor, 3 – *P-type* semiconductor, 4 – *N-type* semiconductor) [13, 17].

Thermoelectric generators are based on elements/cells consisting of P and *N-type* semiconductors. [12]. The materials used in these cells determine their functional performance [13]. The search for new semiconductors that will convert heat into electricity more efficiently is an active research direction in thermoelectric technology [14, 15]. The quantity that characterises the ability of a thermoelectric material to convert energy is the ZT factor [16], which is determined by parameters α_S, ρ_m and λ_m and temperature T.

$$ZT = \frac{\alpha_S^2}{\rho_m \cdot \lambda_m} T, \tag{1}$$

where:
T – absolute temperature of the material, K,
ρ_m – electric resistivity of the material, Ω·m,
λ_m – thermal conductivity coefficient of the material, W/(K·m),
α_S – Seebeck coefficient, V/K.

Examples of ZT efficiency values and the temperature range of the materials are shown in Table 1. Newly developed thermoelectric materials tend to have higher ZT values. They focus on introducing nanomaterials as additives or making them entirely from nanomaterials [11] and non-toxic organic materials [14].

Table 1. Average *ZT* values for different thermoelectric cell materials.

Material	*ZT*	Operating temperature range, °C	Source
$Cu_xSn_1S_4$	0.6	97 ÷ 297	[18]
$Bi_2(Te,Se)_3$ nanowire	1.0	~ 27	[19]
$Bi_{0.5}Sb_{1.5}Te_3$ & $Bi_{0.3}Sb_{1.7}Te_3$	> 1.0	50 ÷ 250	[20]
Bi_2Te_3 nanostructured	> 2.0	–	[21]
$PbTe_{0.7}S_{0.3}$	2.2	400 ÷ 700	[22]

The use of thermoelectric generators as a source of electricity is beneficial and economically justifiable [23]. This source has the advantage of being able to generate electricity directly from a low-temperature heat stream [24]. Such generators are characterised by long life, ability to operate regardless of position in space, noiseless operation [25], vibration resistance, wide operating temperature range, high specific power generation efficiency (W/cm^2), reliability [26], light weight, lack of moving parts, and little to no maintenance requirements [27].

The research on TEG elements aims to improve the thermal-to-electric energy conversion efficiency, which is currently at around 5% (TEC1-12730) for commercial products [26], although values of approximately 10% for Bi_2Te_3 alloys [28] and 11.7 % for $Pb_{1-x}Sb_xTe$ material [29] have been achieved in laboratory systems.

A limitation of the efficiency of thermogenerators is the need to maintain an even temperature distribution on their planes ("hot" and "cold") and a high and constant temperature difference between them, in the range of their work temperature [25]. The disadvantage of these devices is their minimal impact resistance [11].

Single thermoelectric generators, due to the low electric power generated, are used to power low-power electronic components [30–32], such as measurement sensors and simple actuators. Using systems of multiple interconnected thermoelectric generators (TEG batteries), much higher electric power can be generated [23, 33, 34]. To feed it into the public electricity grid, an additional power conversion system (specialised DC/AC converters) is used [35, 36]. Advanced DC/DC converters [37, 38] are applied to directly use the electricity generated in this way.

The paper presents a prototype test bench and a developed two-section module with a battery of thermogenerators. The MTEG module has two prototype sectional heat exchangers and a set of thermogenerators. The novelty of the developed and verified system for measuring the electric parameters of the thermoelectric cell batteries of the section module with thermogenerators lies in the ability to simultaneously measure the generated electric power and the internal resistance of selected TEG elements placed in each of the two sections. The added value of this paper is the developed and discussed research methodology of the MTEG module.

2. Description of the measurement system

The test bench consists of a thermoelectric generator module (Fig. 2), which contains three main components: a *hot-side heat exchanger* (HSHE), thermogenerators, and *a cold-side heat exchanger* (CSHE). Heat $\dot{Q}_{\text{in}}$ is taken up from the HS source by the heat exchanger and then absorbed by the CS source in the form of flux $\dot{Q}_{\text{out}}$. As a result of the heat transfer process, a temperature difference is created on the covers of the thermogenerators, and DC electricity is generated within them. The electricity thus generated can be stored (batteries, capacitors) [39] or converted to a form that meets the user's needs (*e.g.* in wearable multi-sensing and medical applications) [40, 41].

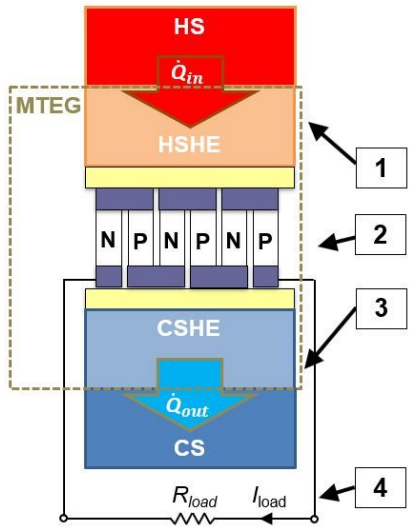

Fig. 2. Thermoelectric current generation circuit in the MTEG module; 1 – high-temperature part; 2 – thermogenerator battery; 3 – low-temperature part; 4 – electric circuit load.

This paper describes a system for measuring the electric parameters of thermoelectric generators consisting of two main sub-systems. One evaluates the internal resistance of individual TEGs and the other measures the electric load parameters of thermoelectric generator batteries. Two generators (Table 2), located in the middle of the individual exchanger sections of the MTEG module (Fig. 3), were selected to assess the internal resistance of the twenty generators connected in series (Table 2). Thermogenerators a_{23} and a_{28}, due to their location in the central parts of the section, operate under the most stable thermal conditions, as do elements a_{13} and a_{18}. However, due to the accessibility of their electrical connections and the thermal insulation of the entire MTEG module, a_{23} and a_{28} were selected for testing as representative systems.

Table 2. Selected thermogenerator parameters [26, 42].

Parameter	Value
Dimensions (height × width × depth) [mm]	62 × 62 × 3.9
Heat exchange surface area of a single side of the module [mm^2]	3844
Maximum electric power from a single module [W]	4.63
Maximum operating temperature [°C]	138
P-N connector (number of thermocouples)	127

The system for measuring the electric parameters of the thermogenerator battery of the MTEG module allows the following to be determined: the electric voltage at individual generators U_{a23} and U_{a28}, the current I_{load} across the electric circuit, and the voltage drop U_{load} across the load resistance (Fig. 4). In the electric parameter measurement system, the individual analogue signals are processed in the A/A (PCB-P1) and A/D conversion sub-systems or directly converted to digital form in the A/D converters of the PLC. The system allows online visualisation of the processed data and its archiving in the PC memory to create knowledge bases.

Metrol. Meas. Syst., Vol. 32 (2025), No. 1, pp. 1–18
DOI: 10.24425/mms.2025.152770

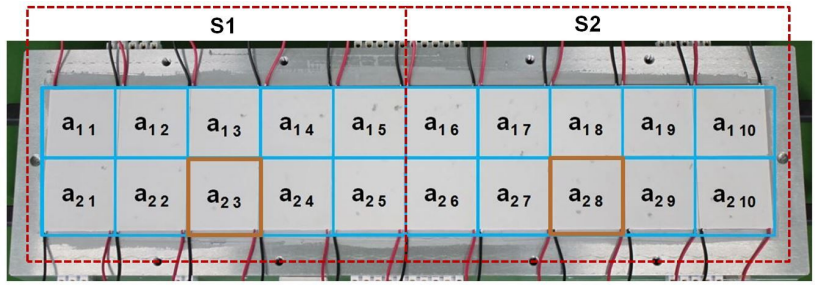

(a)

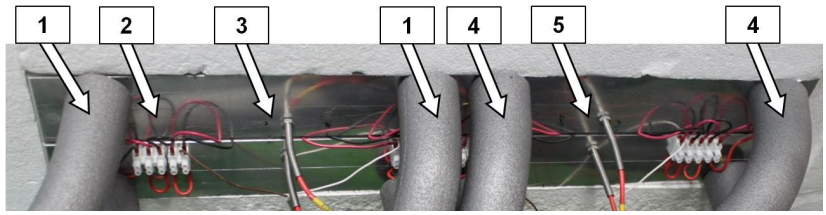

(b)

Fig. 3. View of the test bench – a prototype thermoelectric cell module; a) arrangement of thermogenerator batteries on a two-section heat exchanger (S1 and S2 – exchanger sections); b) view of the MTEG module from electrical and hydraulic connections; 1 – liquid flow connections in Section 1; 2 – TEG electrical connections; 3 – exchanger temperature sensors for Section 1; 4 – liquid flow connections in Section 2; 5 – exchanger temperature sensors for Section 2.

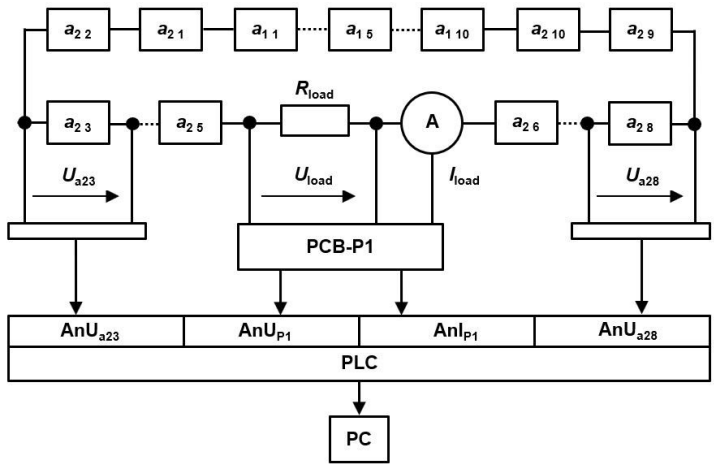

Fig. 4. Block diagram of the measuring system of the thermoelectric battery test module.

The PCB-P1 processing system in a single design solution consists of two electronic analogue converters which process voltage signal U_{load} and current I_{load}, which in turn, are converted to voltage signals (Fig. 5) and routed to the A/D modules (AnU_{P1} and AnI_{P1}). The main processing element in the U_{load} voltage conversion channel is the LV-P1 converter (LV 25-P, *LEM*) [43]. The basic parameters of this element are given in Table 3. Based on this data, the mathematical

formulas in the datasheet [43] and an estimate of the expected voltage on the R_{load}, the values of R_{ZP1} (3.13 kΩ) were selected and the maximum voltage of the measuring range of the converter (U_{load} = 62.6 V ± 0.5 V) was determined. The resistance R_{load} consists of two resistors connected parallelly with an equivalent value of 12.12 Ω (Fig. 6). The measured U_{load} voltage at the input of the measurement system is then converted into an output signal in the system, also in the form of a voltage (at R_{VP1} = 360 Ω), which is further processed in the A/D module (AnU$_{P1}$) of the PLC.

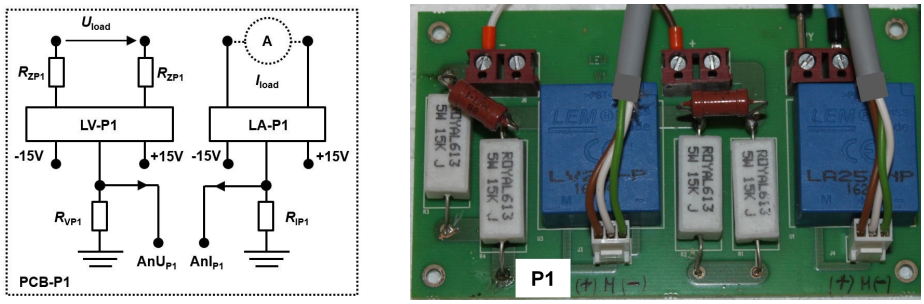

(a) (b)

Fig. 5. PCB-P1 two-channel analogue measurement system; a) scheme; b) prototype PCB board.

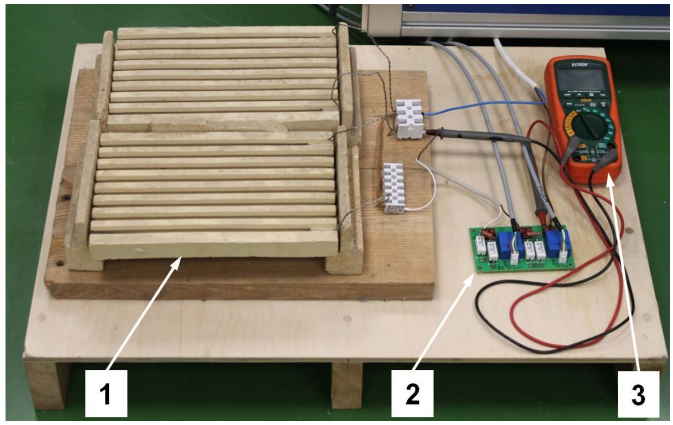

Fig. 6. View of the load resistors of the thermoelectric battery and the two-channel PCB-P1measuring system; 1 – load resistors for the thermogenerator circuit; 2 – PCB-P1 circuit, 3 – current measurement control system.

The element that converts the I_{load} current into electric voltage in the second channel of the PCB-P1 circuit is the LA-P1 converter (LA 25-NP, *LEM*) [44]. Its parameters are given in Table 4. The data from this Table and the estimated value of the current in the thermogenerator circuit (I_{load} = 5.0 A ±0.025 A) allowed us to configure the design of the LA-P1 element of the PCB-P1 circuit. The current intensity measured at the LA-P1 converter input is then converted into a voltage signal (for R_{IP1} = 300 Ω) and into the digital form in the A/D module (AnI$_{P1}$) of the PLC.

Voltage measurement on selected thermogenerators is carried out directly by the A/D modules (AnU$_{a23}$, AnU$_{a28}$) of the PLC (Table 5). Such a measurement is possible due to its low expected value (< 10 V DC) and the electrically isolated design of the analogue measurement module.

Table 3. Selected parameters of the LV 25-P *(LEM)* converter [43].

Parameter	Value
Power supply voltage [V]	±15
Primary rated RMS current (I_{PN}) [mA]	10
Measured voltage DC, AC (U_{PN}) [V]	10 ÷ 500
Secondary nominal current RMS (I_{SN}) [mA]	25
Total error U_{PN} at I_{PN}, t_A = 25°C, ±15 V (±5%) [%]	±0.8
Linearity error [%]	< 0.2
Ambient temperature during operation (t_A) [°C]	0 ÷ 70
Mass [g]	22
Dimensions (height × width × depth) [mm]	15.2 × 26 × 29.2

Table 4. Selected converter parameters LA 25-NP (*LEM*) [44].

Parameter	Value
Supply voltage [V]	±15
Current intensity, AC (I_{PN}) [A]	5 ÷ 25
Secondary rated current RMS (I_{SN}) [mA]	25
Total error at I_{PN}, t_A = 25° [%]	±0.5
Linearity error [%]	< 0.2
Ambient temperature during operation (t_A) [°C]	−40 ÷ 85
Mass [g]	22
Dimensions (height × width × depth) [mm]	16.4 × 26 × 29.2

Table 5. Main parameters of the A/D module of voltage measurement [45].

Name and type	Element description, parameters
Modicon TM5, type: TM5SAI4L (*Schneider Electric*)	– digital resolution of the module: 12-bit – input: −10 ÷ 10 V – module power supply: 20.4 ÷ 28.8 V DC – input impedance: 20 MΩ – input tolerance – maximum deviation at ambient temperature 25°C: < 0.08% measurement – input tolerance – temperature drift: 0.006%/°C measurement – input tolerance – nonlinearity: < 0.025% full scale (20 V DC) – resolution value: 2.441 mV

3. Research method

A procedure for the research method has been developed and is shown in Fig. 7. This algorithm determines the electric parameters of a system with thermogenerators, the total electric power generated, and the internal resistances of two example TEG elements.

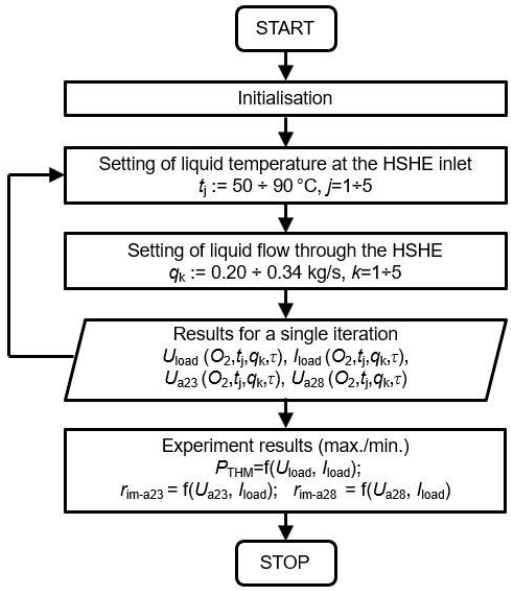

Fig. 7. Experiment procedure.

The first step of the algorithm is initialisation, during which the following parameters are set: the fluid circuits in the hot-side heat exchanger of the thermogenerators (HSHE) to the flow TEG-O2 / O2 (flow inwards), described in detail in the paper [46] and the flow to the right in the cold-side heat exchanger (CSHE) (Fig. 8). In this step, the temperature and flow parameters of the cold liquid of the CSHE are also set.

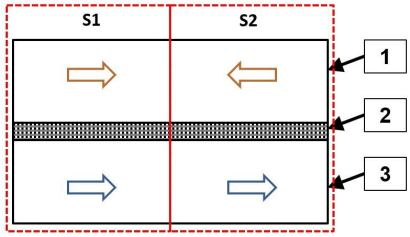

Fig. 8. View of the MTEG module with liquid flow directions in the sections (S) of the exchangers; 1 – HSHE exchanger; 2 – thermogenerator battery layer; 3 – CSHE exchanger.

In the next steps, different setpoint values are selected: temperature t_j in the inlet section of the HSHE exchanger and liquid flow rate q_k. For a given iteration of the test process, the values of the indicated electric parameters are determined (U_{load}, I_{load}, U_{a23}, U_{a28}). The algorithm allows for the execution of a single experiment with a given duration τ, which influences the run length of the iteration loop. The range of variation of a single iteration time was defined as an interval (τ = 15 ÷ 30 min) by measuring the values of the electric parameters of the system with a two-second sampling time. The selection of the duration time is based on the minimum time required to achieve a fixed heat exchange in the MTEG module.

In the last step, the algorithm enables the determination of the minimum and maximum values of the generated electric power P_{THM} and the internal resistance of the two TEG modules ($r_{\text{im-a23}}$, $r_{\text{im-a28}}$).

4. Results of the experiment

Using the algorithm shown in Fig. 7, the operation of the sectional MTEG module and the thermoelectric cell battery electric parameters measurement system was verified. The main electric parameters of the circuit with thermogenerators were determined (U_{load}, I_{load}, U_{a23}, U_{a28}), which made it possible to obtain the values of power P_{THM} and internal resistances $r_{\text{im–a23}}$ and $r_{\text{im–a28}}$. The generated electric power was determined indirectly from the measured electric voltage values U_{load} and current I_{load} from dependence $P_{\text{THM}} = U_{\text{load}} \cdot I_{\text{load}}$. The analysis of the measurement uncertainty, voltage U_{load}, and current I_{load} was conducted for a selection of three variants of the test method (at constant temperature $t_j = 90°\text{C}$ and variable liquid flow q_k).

The test was conducted under stabilised heat transfer conditions for each value of the liquid flow rate. One sample was thirty consecutive observations and the sampling time was two seconds. The results are shown in Table 6.

Table 6. Voltage measurement results U_{load} and current I_{load} for three liquid flow rates q_k.

q_k [kg·s^{-1}]	0.20	0.27	0.34	0.20	0.27	0.34
Parameter	U_{load} (t_j = 90 °C) [V]			I_{load} (t_j = 90 °C) [A]		
Average	18.08	18.30	18.43	1.50	1.52	1.53
Maximum	18.09	18.33	18.45	1.50	1.52	1.53
Minimum	18.06	18.28	18.42	1.49	1.51	1.53
Max. – Min.	0.03	0.05	0.03	0.01	0.01	0.00
$\sigma_{U\text{load}} = u_{U\text{load}}$	0.0019	0.0021	0.0051	–	–	–
$\sigma_{I\text{load}} = u_{I\text{load}}$	–	–	–	0.0003	0.0002	0.0001

Compound uncertainty in the measurement of electric power generated $u_C(P_{\text{THM}})$ was estimated for the data shown in Table 6 and from the mathematical relationship (2) [47].

Figure 9 shows the distribution of measurements U_{load} and I_{load}. They are largely symmetric, unimodal and without extreme outliers. Hence, they can be approximated with the Gaussian distribution [48, 49]. The expanded uncertainty $U_{95}(P_{\text{THM}})$ was determined with a coverage factor adopted of $k_p = 2$ from (3) [48, 49]. Values $U_{95}(P_{\text{THM}})$ at three flow rates q_k are shown in Table 7. The maximum estimated value of the expanded uncertainty in the measurement of the generated electric power was obtained at a flow rate of 0.20 kg·s^{-1} and is $U_{95}(P_{\text{THM}}) = \pm 0.012$ W.

$$u_C\left(P_{\text{THM}}\right) = \sqrt{\left(\frac{\partial P_{\text{THM}}}{\partial I_{\text{load}}}\right)^2 u_{I\text{load}}^2 + \left(\frac{\partial P_{\text{THM}}}{\partial U_{\text{load}}}\right)^2 u_{U\text{load}}^2}, \tag{2}$$

$$U_{95}\left(P_{\text{THM}}\right) = k_p \cdot u_C\left(P_{\text{THM}}\right). \tag{3}$$

Table 7. Extended uncertainties in the measurement of electric power $P_{\text{THM}} = f\,(U_{\text{load}}, I_{\text{load}})$.

q_k [kg·s^{-1}]	0.20	0.27	0.34
Parameter	P_{THM} [W]		
U_{95} (for n = 30)	0.012	0.009	0.006

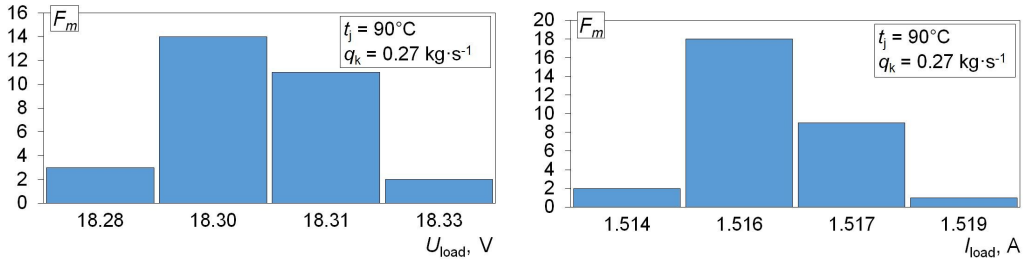

(a) (b)

Fig. 9. Bar charts of sample size U_{load} and I_{load}, conducted at the same temperature.

The maximum estimated expanded uncertainties of measurement of voltage U_{load} and current I_{load} with expansion factor $k_p = 2$ for the data in Table 6 are respectively: $U_{95}(U_{\text{load}}) = \pm 0.01$ V and $U_{95}(I_{\text{load}}) = \pm 0.0006$ A.

The estimated maximum expanded uncertainties were taken as the uncertainties of the measurement sub-systems in question for the presentation of the results: electric power generated, electric voltage U_{load}, and electric current I_{load}. Resistors R_{load} from Kanthal were used as the load. The value of the electrical power dissipated on this load during the tests is small and their operating temperature does not exceed approximately 50°C, hence the determined thermal drift of the resistors is no greater than 0.1%. For this reason, it was decided not to include it in the estimated uncertainty. Examples of the results obtained from the verification of the electrical measuring system U_{load}, I_{load} and P_{THM} circuit with thermoelectric generators, the thermogenerator test module, are shown in Fig. 10.

Internal resistances $r_{\text{im-a23}}$ and $r_{\text{im-a28}}$ were determined by measuring the electric voltages U_{a23} and U_{a28} and current I_{load} in the thermogenerator circuit and then calculated from the relationship: $r_{\text{im-a23}} = U_{\text{a23}}/I_{\text{load}}$ and $r_{\text{im-a28}} = U_{\text{a28}}/I_{\text{load}}$. Uncertainty analysis of parameter measurements U_{a23} and U_{a28} was conducted for three system operating conditions (at constant temperature $t_j = 50$°C and variable liquid flow q_k) with the size ($n = 30$) of a single test sample and a two-second sampling step. The results obtained are shown in Table 8. Compound uncertainty of measurement of internal resistance values $u_C(r_{\text{im-a23}})$ and $u_C(r_{\text{im-a28}})$ was estimated based on the data presented in Table 8, and mathematical relationships (4) and (5). Extended uncertainties $U_{95}(r_{\text{im-a23}})$ and $U_{95}(r_{\text{im-a28}})$ were determined with expansion factor adopted $k_p = 2$ according to (6) and (7). The maximum values of the estimated expanded uncertainties of the measurement of the internal resistance of individual thermogenerators for the individual measurement channels are respectively $U_{95}(r_{\text{im-a23}}) = \pm 0.0008\ \Omega$ and $U_{95}(r_{\text{im-a28}}) = \pm 0.0009\ \Omega$.

$$u_C\left(r_{\text{im-a23}}\right) = \sqrt{\left(\frac{\partial r_{\text{im-a23}}}{\partial I_{\text{load}}}\right)^2 u^2_{I\text{load}} + \left(\frac{\partial r_{\text{im-a23}}}{\partial U_{\text{a23}}}\right)^2 u^2_{U\text{a23}}}, \tag{4}$$

$$u_C\left(r_{\text{im-a28}}\right) = \sqrt{\left(\frac{\partial r_{\text{im-a28}}}{\partial I_{\text{load}}}\right)^2 u^2_{I\text{load}} + \left(\frac{\partial r_{\text{im-a28}}}{\partial U_{\text{a28}}}\right)^2 u^2_{U\text{a28}}}, \tag{5}$$

$$U_{95}\left(r_{\text{im-a23}}\right) = k_p \cdot u_C\left(r_{\text{im-a23}}\right), \tag{6}$$

$$U_{95}\left(r_{\text{im-a28}}\right) = k_p \cdot u_C\left(r_{\text{im-a28}}\right) \tag{7}$$

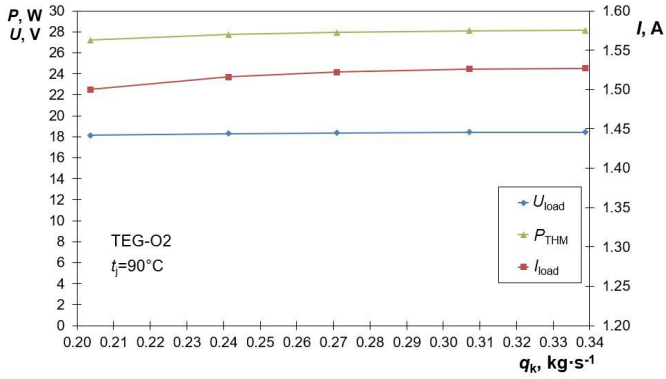

(a)

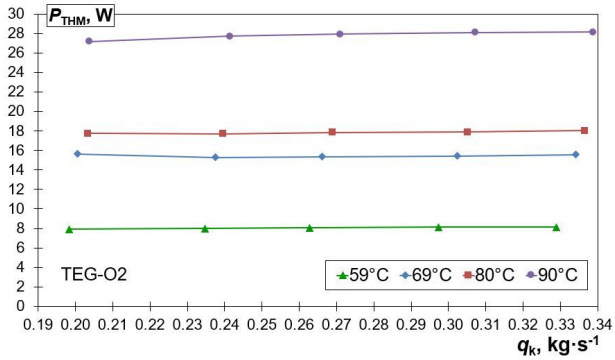

(b)

Fig. 10. Electric power generated P_{THM} as the function of flow rate q_k; a) dependencies P_{THM}, U_{load}, I_{load} for temperature $t_j = 90°\mathrm{C}$; b) power relations P_{THM} for different temperatures.

Table 8. Voltage measurement results U_{a23} and U_{a28} for three flow rates q_k.

q_k[kg·s^{-1}]	**0.21**	**0.29**	**0.31**	**0.21**	**0.29**	**0.31**
Parameter	U_{a23} ($t_j = 50°\mathrm{C}$) [V]			U_{a28} ($t_j = 50°\mathrm{C}$) [A]		
Average	0.465	0.468	0.465	0.454	0.458	0.455
Maximum	0.468	0.470	0.468	0.457	0.460	0.457
Minimum	0.463	0.465	0.463	0.450	0.457	0.454
Max. – Min.	0.005	0.003	0.005	0.007	0.003	0.003
$\sigma_{U\mathrm{a23}} = u_{U\mathrm{a23}}$	0.00025	0.00015	0.00024	–	–	–
$\sigma_{U\mathrm{a28}} = u_{U\mathrm{a28}}$	–	–	–	0.00029	0.00026	0.00028
Parameter	I_{load} ($t_j = 50°\mathrm{C}$) [A]			I_{load} ($t_j = 50°\mathrm{C}$) [A]		
Average	0.735	0.740	0.736	0.735	0.740	0.736
$\sigma_{I\mathrm{load}} = u_{I\mathrm{load}}$	0.00019	0.00017	0.00015	0.00019	0.00017	0.00015

Measurements U_{a23} and U_{a28} presented in Fig. 11 are also quasi-symmetric, unimodal and without outliers, which justifies the use of the Gaussian approximation. Values of estimated uncertainties $U_{95}(r_{\mathrm{im-a23}})$ and $U_{95}(r_{\mathrm{im-a28}})$ at three flow rates q_k are shown in Table 9.

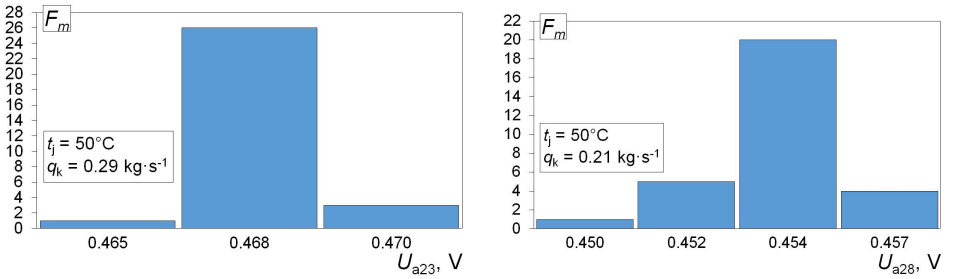

(a) (b)

Fig. 11. Bar charts of sample sizes U_{a23} and U_{a28} for temperature t_j = 50°C.

Table 9. Extended uncertainty of measurement of internal resistances $r_{im-a23} = f\ (U_{a23}, I_{load})$ and $r_{im-a28} = f(U_{a28}, I_{load})$.

q_k[kg·s^{-1}]	0.21	0.29	0.31	0.21	0.29	0.31
Parameter	r_{im-a23} [Ω]			r_{im-a28} [Ω]		
U_{95} (for n = 30)	0.0008	0.0005	0.0007	0.0009	0.0008	0.0008

The maximum estimated expanded uncertainties of measurement of electric voltages U_{a23} and U_{a28} with expansion factor k_p = 2 for the data in Table 8 are respectively: $U_{95}(U_{a23})$ = ±0.0005 V and $U_{95}(U_{a28})$ = ±0.0006 V. Figure 12 shows selected results from the verification process of the parameter measurement system U_{a23}, U_{a28}, r_{im-a23} and r_{im-a28} for the individual TEG elements of the circuit with the thermoelectric generators of the MTEG module.

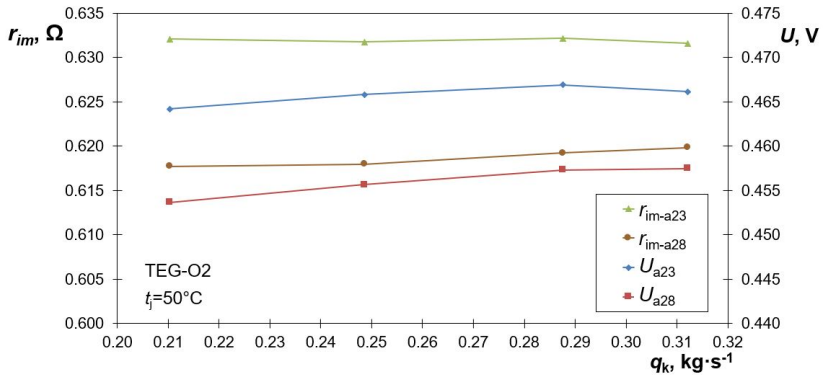

Fig. 12. Internal resistance and electric voltage dependence of individual thermogenerators as the function of the working liquid flow rate.

New measurement systems are subjected to tests that verify their parameters, such as scatter, centring, capability, repeatability, reproducibility, linearity, and stability [50–53]. The repeatability of the EV of the developed measurement system was analysed in accordance with the third procedure of the R&R method [54].

It was determined for each measurement path from two series of twenty-five test trials, with a two-second sampling time. Examples of the results from the analysis of values of the electric parameters measured (U_{load}, I_{load}, U_{a23}, U_{a28}), are shown in Tables 10, 11, 12 and 13.

Quantity σ_Δ and repeatability EV of the measurement system were estimated, with the maximum spread of the analysed parameters and a confidence level of 99%, as given in Tables 6 and 8. The obtained relative repeatability values of the measurement system are in the range $\%EV < 10\%$, hence the developed and verified measurement system is considered "capable" of functioning correctly [54].

Table 10. Summary of procedure parameters for U_{load} using standard deviation.

$\bar{\Delta}$ [V]	s_Δ [V]	σ_Δ [V]	$EV_{0.99}$ [V]	$\%EV_{0.99}$ [%]
–0.004	$1.47 \cdot 10^{-9}$	$1.04 \cdot 10^{-9}$	$5.36 \cdot 10^{-9}$	$1.75 \cdot 10^{-5}$

$\bar{\Delta}$ – arithmetic mean of differences between two series of measurements, s_Δ – standard deviation of the series of differences between measurements, σ_Δ – spread of the measurement system.

Table 11. Summary of procedure parameters for I_{load} using standard deviation.

$\bar{\Delta}$ [A]	s_Δ [A]	σ_Δ [A]	$EV_{0.99}$ [A]	$\%EV_{0.99}$ [%]
–0.0004	$5.38 \cdot 10^{-10}$	$3.80 \cdot 10^{-10}$	$1.96 \cdot 10^{-9}$	$1.09 \cdot 10^{-4}$

Table 12. Summary of procedure parameters for U_{a23} using standard deviation.

$\bar{\Delta}$ [V]	s_Δ [V]	σ_Δ [V]	$EV_{0.99}$ [V]	$\%EV_{0.99}$ [%]
–0.0004	$2.89 \cdot 10^{-5}$	$2.04 \cdot 10^{-5}$	$1.05 \cdot 10^{-4}$	7.01

Table 13. Summary of procedure parameters for U_{a28} using standard deviation.

$\bar{\Delta}$ [V]	s_Δ [V]	σ_Δ [V]	$EV_{0.99}$ [V]	$\%EV_{0.99}$ [%]
0.00008	$4.08 \cdot 10^{-5}$	$2.89 \cdot 10^{-5}$	$1.49 \cdot 10^{-4}$	8.54

5. Conclusions

Measurements of the electric parameters of thermoelectric cell batteries operating in a heat-to-electricity conversion system require high accuracy and repeatability. In the experimental study of the test bench, an MTEG module containing twenty thermogenerators connected in series and constructed from bismuth alloys was evaluated. A research methodology was developed for the thermogenerator module, whose algorithm discussed. The test bench contains several measurement elements including, but not limited to, temperature, liquid flow and pressure sensors, which are necessary to force and monitor thermodynamic processes in the system. This paper presents the verification results of a developed system for measuring the electric parameters of a thermoelectric cell battery of a sectional MTEG module, in which thermogenerators are symmetrically arranged with ten elements in each of the two sections.

Experimental investigations were conducted under thermoelectric cell power generation conditions at varying temperatures and hot liquid mass flow rate measured at the inlet cross-section of the HSHE exchanger and quasi-steady parameters of the heat-taking liquid through the CSHE exchanger.

The current and voltage measurement paths of the load resistance of the serially connected TEG elements and the two, independent internal resistance measurement paths of the selected thermogenerators were checked. The accuracy of the measurement of electric parameters of the

test bench was assessed. The experimental results resembled the Gaussian distribution, with the compound uncertainties of the generated electrical power and the internal resistance of the thermogenerators estimated from the experimental measurements being acceptable.

To achieve the required accuracy of the measurement data, the thermoelectric and thermodynamic phenomena of the module with heat exchangers and thermogenerators had to be analysed under real conditions. It was found that uniform heat transfer across all thermoelectric cells, good matching of the contact surfaces between the walls of the TEG elements and the heat exchangers and the correct strength of their interaction improve the energy conversion efficiency of the thermocells, and the metrological properties of the electric parameters analysed. The use of analogue-to-digital converters with 12-bit resolution was guided by their high A/D data conversion speed and low cost of the measurement modules. The authors strived to design a relatively inexpensive system because, in addition to fulfilling its primary metrological role, it is intended for the multiplication and realization of measurements in complex systems containing dozens or even hundreds of multiplied measuring paths of the presented type.

The developed system for measuring the electric parameters of the cell battery of a sectional module with thermogenerators makes it possible to accurately determine the electric current and voltage and estimate power in an electric circuit as well as measure the internal resistance of the individual TEG elements. The designed measurement paths of the system were subjected to experimental verification and it was found to be suitable for the metrological analysis of the discussed measurement task.

The measurement system in question can be part of a more complex system for controlling the operation of thermoelectric cell batteries and modules with thermogenerators. It allows the electric voltage of a closed and open circuit of a set of thermoelectric generators, as well as the DC currents of the circuit under load and short-circuit conditions to be determined. The system also allows the determination and continuous monitoring of internal resistance of the individual thermogenerators. The above-mentioned measurement capabilities of the system extend its application possibilities to real-time devices for regulating and controlling the maximum output power from TEG batteries, which involves matching (in real time) their internal resistance with an external load [35]. Thus, the prototype system can be used, for example, in controllers operating according to an MPPT (maximum power point tracking) type algorithm [36, 55].

References

[1] Morini, M., Pinelli, M., Spina, P. R., & Venturini, M. (2013). Optimal allocation of thermal, electric and cooling loads among generation technologies in household applications. *Applied Energy*, *112*, 205–214. https://doi.org/10.1016/j.apenergy.2013.05.078

[2] Du, W.-J., Yin, Q., & Cheng, L. (2018). Experiments on novel heat recovery systems on rotary kilns. *Applied Thermal Engineering*, *139*, 535–541. https://doi.org/10.1016/j.applthermaleng.2018.04.125

[3] Atmaca, A., & Yumrutas, R. (2014). Thermodynamic and exergoeconomic analysis of a cement plant: Part II – application. *Energy Conversion and Management*, 79, 799–808. https://doi.org/10.1016/j.enconman.2013.11.054

[4] Karamarković, V., Marašević, M., Karamarković, R., & Karamarković, M. (2013). Recuperator for waste heat recovery from rotary kilns. *Applied Thermal Engineering*, 54, 470–480. https://doi.org/10.1016/j.applthermaleng.2013.02.027

[5] Haddad, C., Périlhon, C., Danlos, A., François, M.-X., & Descombes, G. (2014). Some Efficient Solutions to Recover Low and Medium Waste Heat: Competitiveness of the Thermoacoustic Technology. *Energy Procedia*, *50*, 1056–1069. https://doi.org/10.1016/j.egypro.2014.06.125

[6] Juárez-Huerta, V. H., Sánchez-Salas, N., & Chimal-Eguía, J. C. (2022). Optimization Criteria and Efficiency of a Thermoelectric Generator. *Entropy*, *24*(12), 1812, 1–11. https://doi.org/10.3390/e24121812

[7] Sanin-Villa, D. (2022). Recent Developments in Thermoelectric Generation: A Review. *Sustainability*, *14*(24), 16821, 1–20. https://doi.org/10.3390/su142416821

[8] Khedher, N. B., Selimefendigil, F., Kolsi, L., Aich, W., Said, L. B., & Boukholda, I. (2022). Performance Optimization of a Thermoelectric Device by Using a Shear Thinning Nanofluid and Rotating Cylinder in a Cavity with Ventilation Ports. *Mathematics*, *10*(7), 1075, 1–20. https://doi.org/10.3390/math10071075

[9] Dughaish, Z. (2002). Lead telluride as a thermoelectric material for thermoelectric power generation. *Physica B: Condensed Matter*, *322*(1-2), 205–223. https://doi.org/10.1016/S0921-4526(02)01187-0

[10] Quan, R., Liu, G., Wang, C., Zhou, W., Huang, L., & Deng, Y. (2018). Performance Investigation of an Exhaust Thermoelectric Generator for Military SUV Application. *Coatings*, *8*(1), 45, 1–18. https://doi.org/10.3390/coatings8010045

[11] Zoui, M. A., Bentouba, S., Stocholm, J. G., & Bourouis, M. (2020). Review on Thermoelectric Generators: Progress and Applications. *Energies*, 13, 3606, 1–32.

[12] Meng, J. H., Wang, X. D., & Chen, W. H. (2016). Performance investigation and design optimization of a thermoelectric generator applied in automobile exhaust waste heat recovery. *Energy Conversion and Management*, *120*, 71–80. https://doi.org/10.1016/j.enconman.2016.04.080

[13] Rowe, D. M. (1995). CRC Handbook of Thermoelectrics. *CRC Press LLC*, London.

[14] Kim, M., Park, D., & Kim, J. (2021). Thermoelectric Generator Using Polyaniline-Coated Sb_2Se_3/β-Cu_2Se Flexible Thermoelectric Films. *Polymers*, *13*(9), 1518, 1–11. https://doi.org/10.3390/polym13091518

[15] Twaha, S., Zhu, J., Yan, Y., & Li, B. (2016). A comprehensive review of thermoelectric technology: materials, applications, modeling and performance improvement. *Renewable and Sustainable Energy Reviews*, 65, 698–726. https://doi.org/10.1016/j.rser.2016.07.034

[16] Snyder, G. S., & Snyder, A. H. (2017). Figure of merit ZT of a thermoelectric device defined from materials properties. *Energy & Environmental Science*, 11, 1–6.

[17] Renge, S., Barhaiya, Y., Pant, S., & Sharma, S. (2017). A Review on Generation of Electricity using Peltier Module. *IJERT*, *6*(1), 453–457.

[18] Hasaka, M., Aki, T., Morimura, T., & Kondo, S. I. (1997). Thermoelectric properties of Cu-Sn-S. *Energy Conversion and Management*, *38*(9), 855–859. https://doi.org/10.1016/S0196-8904(96)00098-2

[19] Tan, M., Deng, Y., & Wang, Y. (2014). Ordered structure and high thermoelectric properties of $Bi_2(Te,Se)_3$ nanowire array. *Nano Energy*, *3*, 144–151. https://doi.org/10.1016/j.nanoen.2013.07.009

[20] Pan, Y., Aydemir, U., Grovogui, J. A., Witting, I. T., & others (2018). Melt-Centrifuged $(Bi,Sb)_2Te_3$: Engineering Microstructure toward High Thermoelectric Efficiency. *Advanced Materials*, *30*(34), 1–24. https://doi.org/10.1002/adma.201802016

[21] Mamur, H., Bhuiyan, M. R. A., Korkmaz, F., & Nil, M. (2018). A review on bismuth telluride (Bi_2Te_3) nanostructure for thermoelectric applications. *Renewable and Sustainable Energy Reviews*, *82*(3), 4159–4169. https://doi.org/10.1016/j.rser.2017.10.112

[22] Wu, H., Zhao, L.-D., Zheng, F., Wu, D., & others (2014). Broad temperature plateau for thermoelectric figure of merit ZT>2 in phase-separated PbTe0.7S0.3. *Nature Communications*, *5*, 1–9. https://doi.org/10.1038/ncomms5515

[23] Li, K., Garrison, G., Zhu, Y., Horne, R., & Petty, S. (2021). Cost Estimation of Thermoelectric Generators. *PROCEEDINGS*, 46th Workshop on Geothermal Reservoir Engineering, Stanford University, Stanford, California, 15–17 February, SGP-TR-218, 1–8.

[24] Babu, C., & Ponnambalam, P. (2017). The role of thermoelectric generators in the hybrid PV/T systems: A review. *Energy Conversion and Management*, 151, 368–385. http://dx.doi.org/10.1016/j.enconman.2017.08.060

[25] Wojciechowski, K., Merkisz, J., Fuć, P., & Tomankiewicz, J., & others (2013). Prototypical thermoelectric generator for waste heat conversion from combustion engines. *Combustion Engines*, 154, 3, 60–71.

[26] Jadwiszczak, P., & Sidorczyk, M. (2016). Produkcja energii elektrycznej z ciepła za pomocą ogniw TEG; charakterystyki termoelektryczne termogeneratorów. *Rynek instalacyjny*, 4, 38–42. (in Polish)

[27] Karthick, K., Suresh, S., Muaaz, M., Hussain, M. D., Ali, H. M., & Kumar, C. S. S. (2019). Evaluation of solar thermal system configurations for thermoelectric generator applications: A critical review. *Solar Energy*, *188*, 111–142. https://doi.org/10.1016/j.solener.2019.05.075

[28] Królicka, A., Hruban, A., & Mirowska, A. (2012). Nowoczesne materiały termoelektryczne – przegląd literaturowy. *Materiały Elektroniczne*, *40*(4), 19–34. (in Polish)

[29] Parashchuk, T., Horichok, I., Kosonowski, A., Cherniushok, O., & others (2021). Insight into the transport properties and enhanced thermoelectric performance of n-type $Pb_{1-x}Sb_xTe$. *Journal of Alloys and Compounds*, *860*, 158355. https://doi.org/10.1016/j.jallcom.2020.158355

[30] BioLite, CampStove 2+ Electricity Generating Wood Camp Stove. https://eu.bioliteenergy.com/products/campstove-2-plus. (accessed on 18 May 2024)

[31] Gould, C. A. (2020). Thermoelectric water meter energy harvesting. *Journal of Physics: Conference Series*, IOP Publishing: Bristol, UK, 012010, 1–11. https://doi.org/10.1088/1742-6596/1534/1/012010

[32] Hájovský, R., Pieš, M., & Richtár, L. (2016). Analysis of the Appropriateness of the Use of Peltier Cells as Energy Sources. *Sensors*, *16*(6), 760, 1–13. https://doi.org/10.3390/s16060760

[33] Barma, M. C., Riaz, M., Saidur, R., & Long, B. D. (2015). Estimation of thermoelectric power generation by recovering waste heat from Biomass fired thermal oil heater. *Energy Conversion and Management*, 98, 303–313. https://doi.org/10.1016/j.enconman.2015.03.103

[34] Sztekler, K., Wojciechowski, K., & Komorowski, M. (2016). The thermoelectric generators use for waste heat utilization from conventional power plant. *E3S Web of Conferences*, Energy and Fuels, 14, 01032, 1–8. https://doi.org/10.1051/e3sconf/20171401032

[35] McCarty, R., & Piper, R. (2015). Voltage–current curves to characterize thermoelectric generators. *Journal of Electronic Materials*, 44, 6, 1896–1901. https://doi.org/10.1007/s11664-014-3585

[36] Mrozek, M., Majcher, A., & Neska, M. (2020). Przekształtnik energoelektroniczny do współpracy z generatorami termoelektrycznymi. *Zeszyty Energetyczne*. Wydawnictwo Politechniki Wrocławskiej, VII, 303–314. (in Polish)

[37] Kwan, T. H., & Wu, X. (2017). TEG Maximum Power Point Tracking using an Adaptive Duty Cycle Scaling Algorithm. *Energy Procedia*, *105*, 14–27. https://doi.org/10.1016/j.egypro.2017.03.274

[38] Laird, I., & Lu, D. D. C. (2013). High step-up DC/DC topology and MPPT algorithm for use with a thermoelectric generator. *IEEE Transactions on Power Electronics*, *28*(7), 3147–3157. https://doi.org/10.1109/TPEL.2012.2219393

[39] Champier, D. (2017). Thermoelectric generators: A review of applications. *Energy Conversion and Management*, *140*, 167–181. https://doi.org/10.1016/j.enconman.2017.02.070

[40] Kumar, P. M., Babu, V. J., Subramanian, A., Bandla, A., & others (2019). The Design of a Thermoelectric Generator and Its Medical Applications. *Designs*, *3*(22), 1–26. https://doi.org/10.3390/designs3020022

[41] Wen, D.-L., Deng, H.-T., Liu, X., Li, G.-K., Zhang, X.-R., & Zhang, X.-S. (2020). Wearable multi-sensing double-chain thermoelectric generator. *Microsystems & Nanoengineering*, *6*(1). https://doi.org/10.1038/s41378-020-0179-6

[42] Hebei, I. T. Co., Ltd. Thermoelectric Cooler TEC1-12730 [Datasheet, rev. 2.03]. http://www.hebeiltd.com.cn/peltier.datasheet/TEC1-12730.pdf

[43] LEM International. Voltage Transducer LV 25-P. N°97.27.19.000.0, 8 July 2021/version 20. http://www.lem.com.

[44] LEM International. Current Transducer LA 25-NP. N°97.08.19.000.0, 11 August 2022/version 17. http://www.lem.com.

[45] Schneider Electric. Modicon TM5, Analog I/O Modules, Hardware Guide. [03/2018, EIO0000000450.06].

[46] Neska, M., Mrozek, M., Żurek-Mortka, M., & Majcher, A. (2021). Analysis of the parameters of the two-sections hot side heat exchanger of the module with thermoelectric generators. *Energies*, *14*(16), 5169, 1–15. https://doi.org/10.3390/en14165169

[47] Neska, M., & Majcher, A. (2014). Estimation of the uncertainty of measurement in a two-channel system for tests on the intensity of infrared radiation. *Problemy Eksploatacji – Maintenance Problems*, *3*, 45–55.

[48] EA Laboratory Committee (2022). Evaluation of the uncertainty of measurement in calibration. European co-operation for Accreditation [April 2022 rev03]. https://www.pca.gov.pl

[49] Joint Committee for Guides in Metrology. (2008). Evaluation of measurement data – Guide to the expression of uncertainty in measurement (JCGM 100:2008). http://www.bipm.org/utils/common/documents/jcgm/JCGM_100_2008_E.pdf

[50] Rucki, M., Barisic, B., & Szalay, T. (2008). Analysis of air gage inaccuracy caused by flow instability. *Measurement*, *41*(6), 655–661. https://doi.org/10.1016/j.measurement.2007.10.001

[51] Jermak, C. J., & Rucki, M. (2016). Static Characteristics of Air Gauges Applied in the Roundness Assessment. *Metrology and Measurement Systems*, *23*(1), 85–96. https://doi.org/10.1515/mms-2016-0009

[52] Sałaciński, T. (2012). Analysis of tools and measurement systems capabilities. *Inżynieria Maszyn*, *2*(17), 74–83.

[53] Neska, M. C., & Opara, T. A. (2022). Uncertainty of pressure measurement in a single-bed adsorber. *Metrology and Measurement Systems*, *29*(1), 93–108. https://doi.org/10.24425/mms.2022.138544

[54] Dietrich, E., & Schulze, A. (2010). Statistical Procedures for Machine and Process Qualification. *Hanser Fachbuchverlag*, 6, 1–748.

[55] Benhadouga, S., Meddad, M., Eddiai, A., Boukhetala, D., & Khenfer, R. (2019). Sliding mode control for MPPT of a thermogenerator. *Journal of Electronic Materials*, *48*(4), 2103–2111. https://doi.org/10.1007/s11664-019-06997-y

Mirosław Neska received the Eng. degree from Casimir Pulaski University of Technology, Radom, Poland, in 2002 and the M.Sc. degree from the AGH University of Science and Technology, Krakow, Poland, in 2006. Next, he obtained the Ph.D. degree from Casimir Pulaski Radom University in 2023. He won a scholarship to attend the ICAM Nantes Technical University, France, as part of the Socrates/Erasmus program. He completed an internship as a production quality engineer in the Caillau company, Romorantin, France in 2006. He has been a Senior Specialist in the Control Systems Research Group and a Technical Manager in the Control Systems Laboratory in the Łukasiewicz Research Network – Institute for Sustainable Technologies, Radom, Poland, since 2007. He has authored or coauthored over 35 scientific articles published in Polish and international journals and participated in over 30 Polish and international conferences. His professional interests include control systems, energy systems, renewable energy, programmable systems, measurement systems, metrology, computer process control, and electromagnetic compatibility.

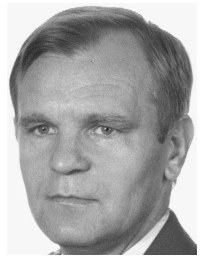

Tadeusz Opara received Ph.D. and D.Sc. from the Military University of Technology, Warsaw, Poland, in 1982 and 1997. He received the title of Professor at the Rzeszów University of Technology, Poland, in 2012. He used to be a Full Professor at the Faculty of Mechanical Engineering of the University of Technology and Humanities in Radom, Poland. He has authored 2 books and over 70 journal publications. His interests include physical properties of liquid crystals, diffraction methods for studying the spray spectrum of fuel aerosols, composite ablative materials, posturography studies of pilots, and thermodynamic issues.